Numerical and Experimental Investigations of Reinforced Masonry Structures across Multiple Scales

Eleni N. Chatzi, Savvas P. Triantafyllou and Clemente Fuggini

Abstract This review chapter outlines the outcomes of a combined experimental-numerical investigation on the retrofitting of masonry structures by means of polymeric textile reinforcement. Masonry systems comprise a significant portion of cultural heritage structures, particularly within European borders. Several of these systems are faced with progressive ageing effects and are exposed to extreme events, as for instance intense seismicity levels for structures in the center of Italy. As a result, the attention of the engineering community and infrastructure operators has turned to the development, testing, and eventual implementation of effective strengthening and protection solutions. This work overviews such a candidate, identified as a full-coverage reinforcement in the form of a polymeric multi-axial textile. This investigation is motivated by the EU-funded projects Polytect and Polymast, in the context of which this protection solution was developed. This chapter is primarily concerned with the adequate simulation and verification of the retrofitted system, in ways that are computationally affordable yet robust in terms of simulation accuracy. To this end, finite element based mesoscopic and multiscale representations are here overviewed and discussed within the context of characterization, identification and performance assessment.

Eleni N. Chatzi
Institute of Structural Engineering, ETH Zürich, Stefano-Franscini-Platz 5, 8093, Zurich, Switzerland, e-mail: chatzi@ibk.baug.ethz.ch

Savvas P. Triantafyllou
Centre for Structural Engineering and Informatics, The University of Nottingham, University Park, NG7 2RD, UK e-mail: Savvas.Triantafyllou@nottingham.ac.uk

Clemente Fuggini
Industrial Innovation Division, DAppolonia S.p.A., Via San Nazaro 19, 16145 Genova, Italy e-mail: clemente.fuggini@dappolonia.it

1 Introduction

In recent years awareness has been raised among both engineers and authorities on the importance of shielding infrastructure against extreme events, such as earthquakes, particularly with respect to those items that form part of our cultural heritage. Recent pronounced catastrophes associated with the earthquakes in Tohoku (2011), Christchurch (2011), Modena (2012) and Central Italy (2016), formed a wake up call regarding the potential impact of such events in terms of material damage and, more importantly, human loss. Societies have since turned towards the notion of resilience, which encourages the search for new materials and methodologies able to strengthen and protect structures against natural hazards, including seismicity.

Masonry is a composite material comprising distinct units of various natural or industrial materials e.g. stone, brick, concrete etc. [1, 2]. The constituents usually demonstrate a brittle and in general anisotropic behavior in a micro-level. The latter eventually propagates to the macro-level [3, 4, 5, 6], and is further enhanced by inherent "weak" planes along the head and bed joints, leading to in- and out-of-plane failure mechanisms, which are often activated by seismic loading. The prevention of structural collapse due to seismic events, and the enhancement of structural integrity, are still open points of discussion within the scientific community as a number of different techniques may be considered suitable, depending on the characteristics of the input load.

Masonry structures comprise an essential feature of global infrastructure heritage. Many of these structures however, have not necessarily been designed against seismic loads, but rather with the primary goal of withstanding gravity loads [7]. Nonetheless, underestimation of the effects of seismicity may be detrimental, particularly when associated with increased in-plane and out-of-plane forces, which may ultimately lead to failure [8]. To accurately simulate the behavior of masonry, a thorough accounting of the damage and failure mechanisms need be put in place. To this end, effective nonlinear modeling tools are essential, albeit often laborious to establish, owing to the inherent complexity in either the local (constituents) or global (system) level.

For alleviating collapse and failure incidents, retrofitting techniques have been proposed that are particularly suited for the special class of masonry structures. Standard methods of intervention include strengthening through external pre-stressing [9], externally bonded strips or overlays [10], and near-surface mounted reinforcement [11]. During recent years however, textile composites have surfaced as an effective means for the retrofitting and strengthening of reinforced concrete and masonry structures [12]. As opposed to other fiber-based materials such as Fiber Reinforced Polymers (FRPs) that are implemented onto masonry as a set of individual strips, textile materials are produced as fabric meshes of fibre rovings in at least two directions. As such, textile composites provide wide area coverage, can prevent falling debris, help distribute loads, are low-cost, easy to apply, provide a high strength to weight ratio, are resistant to electro-chemical corrosion, are non-invasive, are fatigue resistant, are non-magnetic, and have the potential to reduce

seismic retrofitting costs. Such composite materials in the form of sheets or wrappers, have been been implemented for the effective strengthening of masonry structures [13, 14].

Textile solutions are often implemented in strips of fiber reinforced composites (carbon or glass fibers), which are attached via adhesive (resin) onto localized areas of the wall (CNR-DT 200/2004) [15]. A shortcoming to this approach lies in the potential local increase of stiffness leading to undesired stress concentrations and an unfavorable redistribution of dynamic loads. A remedy to this approach, in the form of a full coverage solution, has been tested and validated within the context of the EU funded project Polytect - Polyfunctional Technical Textiles for Protection against Natural Hazard [16, 17, 18]. The purpose of implementing a full coverage solution as in the case of composite textiles is two-fold. First of all, the system acts as a mechanical adhesive bridging cracks that may exist on the body of the masonry. Although each individual fiber demonstrates brittle material behavior with an elastic branch until failure, the overall behavior of the textile is ductile as failure propagates in a successive manner during cyclic loading. As a result, textiles significantly increase the ductility and shear strength of retrofitted masonry, while additionally achieving an improved load distribution. Finally, an added advantage to this solution is delivered via its embedded monitoring technology enabled via Fibre Optical strain sensors. Monitoring of these solutions is further suggested by the European guidelines (CNR-DT 200/2004), as a consequence of the reduced knowledge base available and rather limited experience gathered regarding their long–term behavior.

The use of testing and the subsequent extraction of structural feedback in the form of measurements, allows for enhancing current understanding on such complex systems. When investigated within a laboratory setting, a number of mixed numerical-experimental techniques have been proposed for simulation and verification of polymer reinforcing materials [19, 20, 21]. On the other hand, and as was originally conceived in the Polytect project, structural feedback may also be obtained from structures in-operation via use of appropriate sensors. In both cases, it is only via coupling of the recorded information with an appropriate structural model that the info stemming from raw measurements may be transcribed into meaningful insight regarding the condition and behavior of the system.

This is commonly achieved with an inverse problem setting, where response response observations serve as the starting point of an iterative procedure for identifying the underlying structural properties of the investigated system. However, when discussing retrofitting solutions for the purpose of seismic protection, it becomes evident that availability of measurements from dynamic loads or seismic events is of particular importance. The latter naturally necessitates a nonlinear dynamic analysis, which nonetheless comes at increased computational costs with obvious drawbacks when cast in an inverse problem setting. It is therefore imperative to develop and employ model structures that are adept in counterpoising the desired level of precision with the associated computational cost.

This paper provides a review of methods available for the modeling and characterization of retrofitted masonry systems. The Polytect project is exploited as a reference case-study for demonstrating the steps that are necessary for the monitoring,

simulation and verification of protection solutions for cultural heritage structures. In a first step, we demonstrate the use of Finite-Element based models of diverse fidelity, and their inverse calibration via heuristic approaches, with a Genetic Algorithm serving as the optimization tool. The procedure proves successful, albeit severely draining in terms of both computational power and time. In a second stage, this review paper demonstrates how a multiscale analysis scheme can enhance the computational efficiency of numerical simulation tools, while retaining their level of refinement. The latter results in a dramatic acceleration of the problem solution, which can be exploited in the context of demanding tasks such as identification, uncertainty quantification and reliability assessment.

2 State-of-the-Art in Simulation

2.1 Masonry Modeling

The modeling of materials that are multi-phase in nature is a non-trivial one. Masonry is a composite material whose diverse constituents exhibit an anisotropic and in general brittle microscopic behavior. The anisotropy at the micro level together with the inherent weak directions along joints results in a highly anisotropic macroscopic behavior [3]. This anisotropy is also influenced by the spatial distribution of the joints, as well as the mechanical properties of the mortar. An immediate consequence of this anisotropy is the fact that the bending strength of a masonry wall varies significantly when in-plane or out-of plane bending is considered [22]. Furthermore, fabrication and construction processes invoke notable variability of the mechanical properties [23].

It is therefore apparent that depending on the problem-at-hand, and the particular goal of the simulation study, appropriate modeling tools and corresponding assumptions should be adopted. Three are the main modeling approaches in the modeling of masonry response, namely micro-models, macro-models and multiscale models (Figure 1). Macro-modeling is a phenomenological approach where the response of a structural element, e.g. wall, rather than the response of its constituents is examined. In macro-modeling masonry is treated as a continuum with smeared material properties. To account for different properties along the main axes of the element, the material is regarded as an anisotropic composite and a relationship is established between generalized stress and strain measures. In the case of masonry, an accurate macro-model must reproduce an orthotropic material with different tensile and compressive strengths along separate material axes. Several macro-elements have been proposed to such an end [24, 25, 26]. Relatively recently, Chen et al. [27] developed a macro-element for the in-plane nonlinear analysis of unreinforced masonry piers.

On the other hand, refined masonry models (micro-models) include a distinct representation of the separate constituents, i.e., units (bricks), mortar and the brick/mortar interface, with fusion of continuum and discontinuous elements. The units (bricks)

are often represented by continuum elements, while discontinuous elements approximate the behavior of joints and interfaces. Each joint, consisting of mortar and the two unit-mortar interfaces, is lumped into an "average" interface, while the units are expanded in order to keep the geometry unchanged.

Due to their obvious computational advantages, as opposed to more refined approaches, macro-modeling procedures are practically the only computational tool implemented at the design office. However the associated macro-modeling parameters need to be properly identified for providing acceptable results. This calibration is usually based on actual experimental data that is hard to secure and usually comes at a high cost. In alleviating these issues, the multiscale method offers a compromise between the macro- and micro-approach, and is in this work presented as a viable alternative.

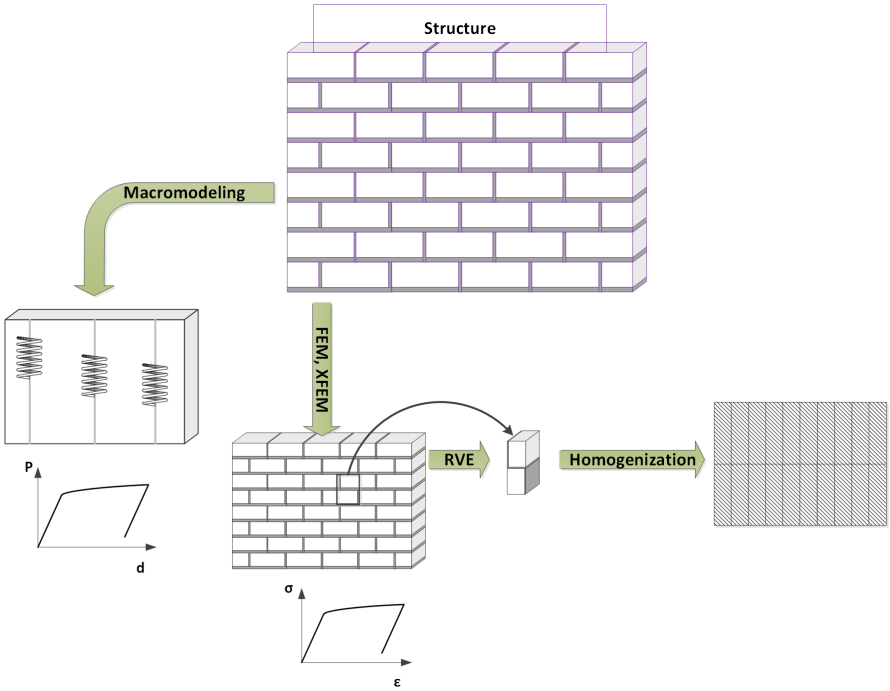

Fig. 1: Different modeling approaches for the structural analysis of composite structures.

2.2 Multiscale Modeling

Multiscale modeling is a rigorous mathematical approach for the scaling of complex numerical problems, significantly reducing the required computational cost [28]. Multiscale and homogenization schemes [29] are commonly adopted in the modeling of materials whose macroscopic behavior is influenced by, and dependent upon, changes in the micro-structure, e.g. granular [30] or cellular and honeycomb materials [31, 32]. In terms of constitutive modeling, multiscale methods have proven their versatility and accuracy where complex plasticity behaviors are observed [33]. The major benefit of multiscale methods lies in their ability to significantly enhance the computational performance of conventional computational mechanics schemes, such as the Finite Element Method. This feature justifies their popularity in a broad spectrum of implementation domains, from molecular-mechanics to computational mechanics [34, 35, 36, 37].

Considerable work has been performed in this field with respect to the modeling of composites, see e.g. [38, 39, 40]. Massart et al. [41, 42] have developed a meso-scale constitutive model for masonry that accounts for anisotropic plasticity effects and damage of the constituents by implementing a generalized plane-stress state assumption. However, multiscale schemes relying on homogenization place the rather limiting assumption of periodicity not only of the micro-structure, but additionally to what concerns damage propagation throughout the macro-scale. A further assumption is placed concerning the full separation of the micro and macro scales considered. These limiting assumptions are eliminated in the multiscale finite element method (MsFEM) introduced by Efendiev and Hou [43]. In [44] an enhanced multiscale finite element (EMsFEM) scheme is presented that extends the applicability of the classical MsFEM into the realm of nonlinear mechanics. The work presented here builds upon this latter method, and extends it for implementation with problems of nonlinear plasticity.

2.3 Smooth hysteretic modeling

Like cementitious materials, masonry too is only adept in the handling of compression, with limited capabilities in the tensile or shear fronts. It further exhibits orthotropic behavior in directions that lie parallel and orthogonal to the mortar joints. In developing a model able to account for the resulting nonlinear behavior, a multiplicity of effects need be taken into account including cracking, crushing, tension softening, compression softening and shear transfer across crack slips. Naturally, the modeling task becomes more complex when moving from monotonic to cyclic or dynamic loads, since nonlinearity is then linked to energy dissipation and hysteresis, with manifestation of stiffness degradation and strength deterioration effects. In tackling this issue from a macroscopic perspective, Karapitta et al. [45] employ a smeared-crack approach for the modeling of unreinforced masonry walls, while

Lourenço [25] introduced a model relying on plasticity theory for the modeling of masonry walls loaded in-plane.

From a microscopic perspective, on the other hand, a hysteretic finite element formulation may be adopted relying on the concept of smooth hysteretic models, such as the Bouc-Wen model [46] or Preisach type models [47]. As illustrated in Figure 2, the Bouc-Wen model in particular tackles the representation of hysteresis via superposition of an elastic (1) and a hysteretic (2) component, corresponding to an elastic stress component σ_{el} and a hysteretic stress component σ_h. Furthermore, the strain corresponding to the hysteretic spring is established in terms of total strain, ε, and slip on the slider, x. Incorporation of hysteretic finite elements enables a more robust and computationally efficient formulation, able to represent the full hysteretic response cycle, which is particularly suited for nonlinear dynamic analysis. Furthermore, smooth hysteretic models are capable of compactly simulating damage-induced phenomena, including stiffness degradation, strength deterioration and pinching [48, 49]. Due to their robust mathematical background, implementation of smooth hysteretic laws has been proven to yield computationally efficient formulations in different disciplines, ranging from solid physics and ferromagnetism [50, 51] to stochastic engineered systems [52], and to hysteretic finite element schemes [53] with the latter demonstrated in what follows.

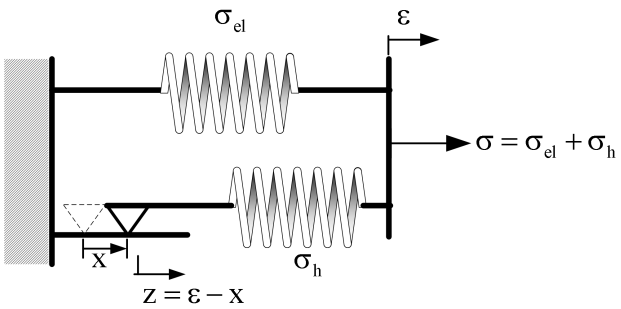

Fig. 2: The Bouc Wen Model: additive decomposition of the elastic and hysteretic component.

3 The Hysteretic Multiscale Finite Element Method (HMsFEM)

In coupling the capabilities offered by the state-of-the-art formulations overviewed previously, Triantafyllou & Chatzi [54] have proposed the Hysteretic Multiscale FEM (HMsFEM) formulation, which merges the computational multiscale scheme with the implementation of the hysteretic finite elements in the micro-scale.

3.1 The Enhanced Multiscale Formulation (EMsFEM)

A computational multiscale approach is utilized in this review paper, namely the Enhanced Multiscale Finite Element method (EMsFEM) introduced in [44]. The method exploits patterns of periodicity present at the micro-scale level for grouping sets of micro-elements into clusters, herein referred to as Representative Volume Elements or RVEs (macro-elements). A visualization is offered in Figure 3, where the coarse RVEs are indicated in subfigures 3(c) and 3(d). Discretization on the basis of the RVEs defines a mesh that is significantly coarser than the respective micro-scale mesh. The benefit of the EMsFEM approach lies in the redefinition of the space where governing equations are solved, shifting the analysis from the fine mesh of Figure 3(a) to the coarser mesh of Figure 3(e). To this end, it is useful to distinguish between the micro- and macro-scale via use of an appropriate notation; $\mathbf{u_m}$ will be used to denote the displacements at the micro-nodes, while $\mathbf{u_M}$ stands for the macro-displacement field. As in the standard finite element context, it is possible to interpolate the micro-displacement vector at the nodes by using an interpolation scheme as in [55]. For a hex-element this would imply:

$$\mathbf{u_m} = [N]_m d_m^i \quad where \quad d_m^i = \underbrace{\left\{ u_{m(1)} \; v_{m(1)} \; \cdots \; v_{m(8)} \right\}^T}_{1x24} \tag{1}$$

is the vector of nodal displacements of the i_{th} micro-element, and $[N]_m$ is the interpolation matrix of the hex-element.

The RVEs also comprise hex-elements whose nodal displacements may be aggregated in the following macro-displacement vector:

$$d_M^i = \underbrace{\left\{ u_{M(1)} \; v_{M(1)} \; \cdots \; v_{M(8)} \right\}^T}_{1x24} \tag{2}$$

where (i) designates the i_{th} macro-node of the coarse (RVE) mesh. In what follows, m will be used to designate components at the micro-scale, while M will be used to designate components at the macro-scale.

For transitioning from the micro- (1) to the macro-scale (2), a mapping is constructed relying on suitable basis functions. In matrix form this is established as:

$$\{d\}_m = [N]_m \{d\}_M \tag{3}$$

where $\{d\}_m$ is the $(3n_{micro} \times 1)$ vector of the micro-mesh nodal displacements, $[N]_m$ is the micro-basis shape function matrix evaluated at the nodes of the micro-mesh (x_j, y_j, z_j), while $\{d\}_M$ is the vector of the macro-node displacements. Per the standard definition of shape function, each column of $[N]_m$ represents a deformed configuration of the RVE, with a value of unit at the corresponding macro-degree of freedom, and null values at the remaining macro-degrees of freedom.

The micro-basis functions occur via solution of the following boundary value problem:

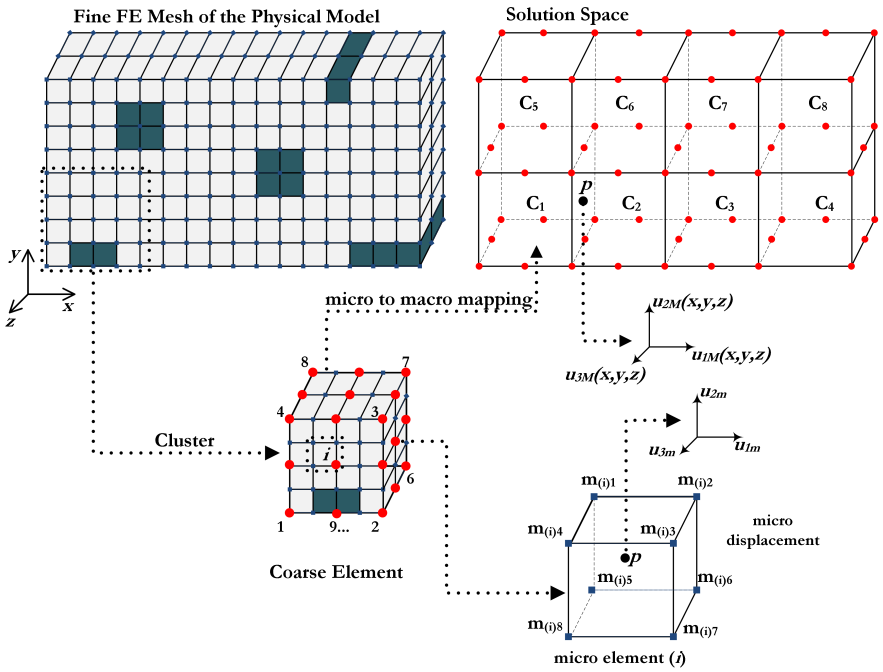

Fig. 3: The MsFE modeling scheme

$$\begin{aligned} [K]_{\mathrm{RVE}}\{d\}_m &= \{\emptyset\} \\ \{d\}_S &= \{\bar{d}\} \end{aligned} \tag{4}$$

where $[K]_{RVE}$ designates the RVE stiffness matrix, $\{d\}_S$ is the vector of degrees of freedom along the boundary S of the RVE, and $\{\bar{d}\}$ is a predefined displacement vector. Different options are available for specifying the boundary conditions, a feature critical to the performance of the method, including the linear, periodic and oscillatory boundary conditions, as elaborated upon in [43, 44].

3.2 The Hysteretic Multiscale Formulation (HMsFEM)

This Section offers a brief overview of the HMsFEM scheme, however the interested reader is referred to [56, 57] for further details on this formulation. The hysteretic feature of the formulation relies on the additive decomposition of the total strain into a reversible elastic and an irreversible inelastic component [58] (Figure 2):

$$\{\dot{\varepsilon}\}_{m(i)} = \left\{\dot{\varepsilon}^{el}\right\}_{m(i)} + \left\{\dot{\varepsilon}^{pl}\right\}_{m(i)} \tag{5}$$

where $\{\varepsilon\}_{m(i)}$ is the total strain tensor, $\left\{\varepsilon^{el}\right\}_{m(i)}$ is the tensor of the elastic, reversible, strain and $\left\{\varepsilon^{pl}\right\}_{m(i)}$ denotes the tensor of plastic strains, while $m(i)$ indexes the i_{th} micro-element within the RVE. The $(.)$ symbol denotes a time-derivative. The isoparametric interpolation scheme is here considered for the displacement field

$$\{d\}_{m(i)} = [N]\{u\}_{m(i)} \tag{6}$$

where $[N]_{m(i)}$ is the shape function matrix. The corresponding strain-displacement relationship is inferred on the basis of compatibility [55] as:

$$\{\varepsilon\}_{m(i)} = [B]\{u\}_{m(i)} \tag{7}$$

where $[B]$ is the strain-displacement matrix.

Moreover, the interpolation scheme defined for plastic deformations assumes the form:

$$\left\{\dot{\varepsilon}^{pl}\right\}_{m(i)} = [N]_e \left\{\dot{\varepsilon}^{pl}_{cq}\right\}_{m(i)} \tag{8}$$

where $\left\{\varepsilon^{pl}_{cq}\right\}_{m(i)}$ denotes the strain vector evaluated at appropriately defined points (collocation points) and $[N]_e$ is the respective interpolation matrix.

By plugging equation (5) into the Principle of Virtual Work [59], and via use of the former interpolation schemes, it is straightforward to derive the elastic $\left[k^{el}\right]_{m(i)}$ and hysteretic $\left[k^{h}\right]_{m(i)}$ stiffness matrices:

$$\begin{aligned} \left[k^{el}\right]_{m(i)} &= \int_{V_e} [B]^T [D]_{m(i)} [B]\, dV_e \\ \left[k^{h}\right]_{m(i)} &= \int_{V_e} [B]^T [D]_{m(i)} [N]_e\, dV_e \end{aligned} \tag{9}$$

The governing equation of the problem may then be written as:

$$\left[k^{el}\right]_{m(i)} \{\dot{d}\}_{m(i)} - \left[k^{h}\right]_{m(i)} \left\{\dot{\varepsilon}^{pl}_{cq}\right\}_{m(i)} = \frac{1}{v_\eta} \{\dot{f}\}_{m(i)} \tag{10}$$

where v_η is a degradation parameter, which increases with plastic deformation (reference value equals 1 for no yielding, see [60] for further details). It need be mentioned that both $\left[k^{el}\right]_{m(i)}$ and $\left[k^{h}\right]_{m(i)}$ are constant matrices. The evolution of plastic deformations, and thereby nonlinearity, is evaluated at the Gauss points of the corresponding micro-scale element, and is defined as:

$$\left\{\dot{\varepsilon}^{pl}\right\}_{m(i)} = \mathscr{F}\left(\left\{\varepsilon^{el}\right\}_{m(i)}, \left\{\dot{\varepsilon}^{el}\right\}_{m(i)}, \{\sigma\}_{m(i)}\right) \tag{11}$$

where $\mathscr{F}$ is a hysteretic operator [50, 61, 62]. A multi-axial Bouc-Wen type smooth plasticity model [63] is herein adopted as the aforementioned operator. The benefit of employing such a rule is that the nonlinear behavior may be accounted for in a

compact representation, fully governed by a finite set of parameters; the parameters of the hysteretic model. Figure 4 exemplifies how a typical hysteretic loop may be accounted for via adoption of an appropriate yield flow rule Φ and a kinematic hardening rule, further regulated by the plastic multiplier $\dot{\lambda}$, as described in the work of [64]. For further details, the interested reader is referred to [60].

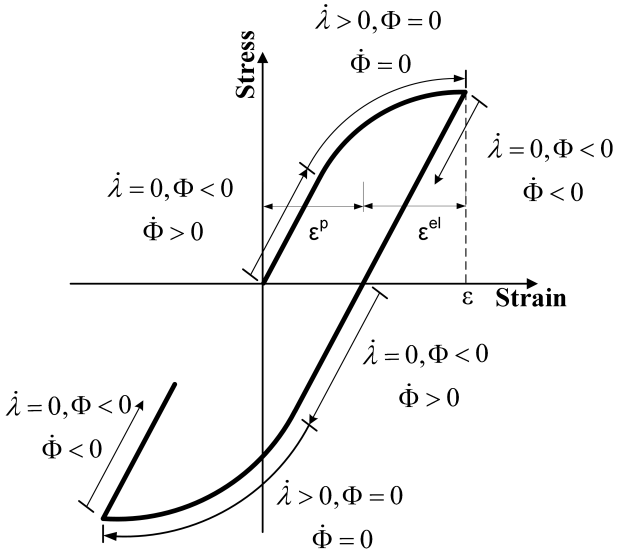

Fig. 4: The classical plasticity loop accounted for by the Bouc Wen model.

The smooth hysteretic model additionally offers the potential of including damage induced phenomena such as damage degradation, strength deterioration and pinching, as elaborated upon in [65, 48]. Table 1 summarizes the defining parameters of the smooth hysteretic model, with details on the corresponding formulations found in [54].

Table 1: Smooth Hysteretic Model Parameters

Effect	Parameter
Hysteretic Shape	β, γ, N
Deterioration	c_η (stiffness), c_s (strength)
Pinching	ζ_1^0, ψ_0, δ_ψ, μ, p, q

Next, by following the reasoning adopted under the EMsFEM scheme, it is possible to demonstrate [54] that the RVE equilibrium equation now assumes the following form:

$$[K]^{M}_{RVE(j)}\{d\}_{M} = \{f\}_{M} - \{f_h\}_{M} \tag{12}$$

where $[K]^{M}_{RVE(j)}$ is the RVE stiffness matrix derived as:

$$[K]^{M}_{RVE(j)} = \sum_{1}^{i} \left[k^{el}\right]^{M}_{m(i)} \tag{13}$$

while $\{f\}_{M}$ is the nodal force vector, comprising mapped contributions from the micro-nodal force components:

$$\{f\}^{M}_{m(i)} = \frac{1}{v_\eta}[N]^{T}_{m(i)}\{f\}_{m(i)} \tag{14}$$

and $\{f_h\}_{M}$ is the plastic force vector evaluated as:

$$\{f_h\}_{M} = \sum_{i=1}^{m_{el}} \left[k^{h}\right]^{M}_{m(i)} \left\{\varepsilon^{pl}_{cq}\right\}_{m(i)} \tag{15}$$

Equation (12) occurs through the principle of energy equivalence between the deformation energy of the RVE and the corresponding micro-mesh [54]. The major benefit of this approach versus standard multiscale schemes, is that the recalculation of the micro-basis functions, which would be required every time the structure shifts from the elastic to plastic regimes, is no longer necessary. Instead, the micro-basis functions are now calculated only once in the beginning of the analysis, while the employed smooth hysteretic law accounts for the evolution of nonlinearity.

The direct stiffness method is then implemented for casting the governing equation of the dynamic problem in the macro-level:

$$[M]\left\{\ddot{U}\right\}_{M} + [C]\left\{\dot{U}\right\}_{M} + [K]\{U\}_{M} = \{P\}_{M} \tag{16}$$

The nodal load vector $\{P\}_{M}$ for the RVE mesh $(ndof_M \times 1)$ in Equation (16) occurs as:

$$\{P\}_{M} = \{F\}_{M} + \{F_h\}_{M} \tag{17}$$

where $\{F\}_{M}$ is the $(ndof_M \times 1)$ external loads vector and $\{F_h\}_{M}$ is the $(ndof_M \times 1)$ hysteretic load vector at the global level. $[M]$, $[C]$ and $[K]$ designate the $(ndof_M \times ndof_M)$ mass, viscous damping and elastic stiffness matrices, which are evaluated at the RVE mesh (macro-scale).

The solution of the global equations of motion is therefore carried out at the macro-scale. This in turn implies that the resulting macro-displacements $\{U\}_{M}$ should be downscaled (mapped to the micro-scale) in order to derive the corresponding local strains. The computational aspects of the HMsFEM overviewed herein are offered in detail in [54].

4 Case Study - Polymeric Textiles for Seismic Retrofitting of Masonry

Within the framework of the Seismic Engineering Research Infrastructures for European Synergies (Series) initiative (http://www.series.upatras.gr, Polymast 2011) and as part the EU co-funded projects Polytect [66] and Polymast [17], textile reinforcement solutions have been developed. These were tested under full-scale seismic tests carried out in the European Center for Training and Research in Earthquake Engineering (Eucentre). As part of the conducted experimental campaign, a previously damaged unreinforced two storey stone building served as a reference case-study for assessment of a "seismic wallpaper" reinforcing solution (Figure 5). The purpose was to establish a benchmark for the retrofitting and repair of masonry-type structures, which have been damaged due to seismic events. The building's dimensions along the length, width and height were 5.80m x 4.40m x 5.80m respectively. It features concrete foundation, a wooden roof and a wooden first-storey slab.

Fig. 5: 3D View of the unreinforced (left) and reinforced (right) stone building, reproduced from [66, 17].

While still in the unreinforced (URB) stage, the structure was tested under dynamic loads on a shake-table until damage. Preliminary repairs were performed through filling of cracks with epoxy resin and stiffening of the wooden slab. The damage-repaired building (DRB) was again non-destructively tested and subsequently reinforced via application of a full-cover solution, namely a composite seismic wallpaper. The composite wallpaper (polymeric textile), which is illustrated in Figure 6, features the following components:

1. Multiaxial, warp-knitted, Alkali Resistant (AR)-glass and Polypropylene (PP) fibers
2. Nanoparticle enhanced coatings for the polymeric textile; Nanoparticle enhanced mortar for ensuring the bond to the protected structure.

3. Fiber optic strain sensors embedded into the textile, with dynamic sampling capability up to 1 kHz.

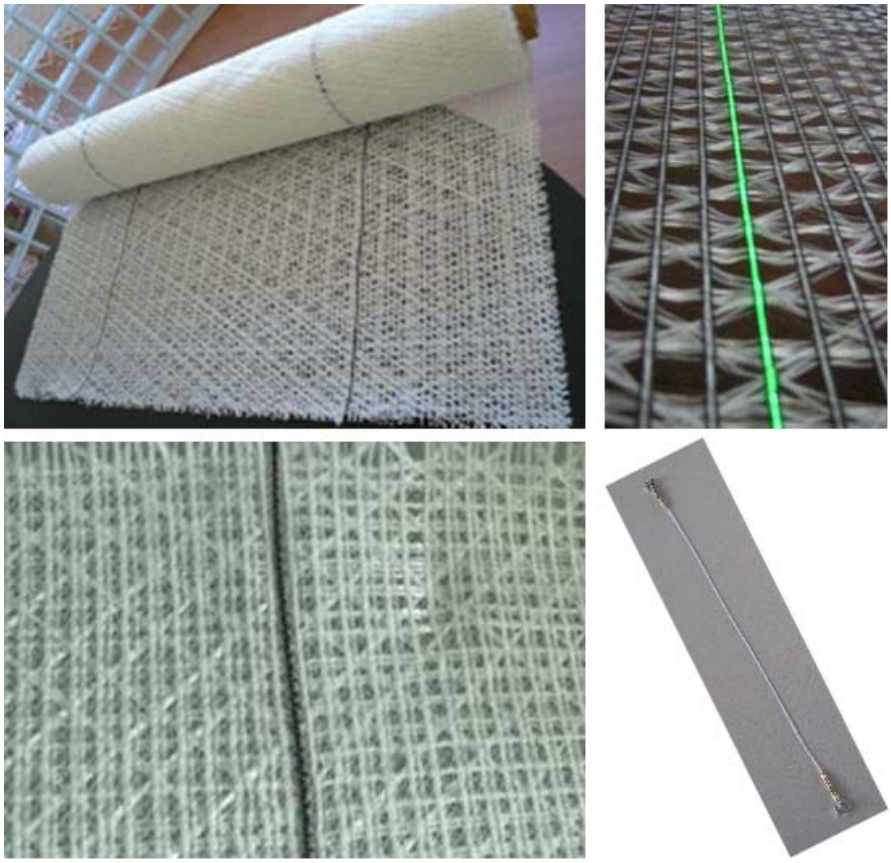

Fig. 6: Composition of the quadri-axial polymeric textile employed as a full-coverage seismic protection, reproduced from [66, 17].

An epoxy mortar compound ensured an almost perfect bond between the textile and the masonry structure; an assumption which was later experimentally validated. This further allows for simplification of the adopted numerical analysis alleviating the necessity for assumptions on interface/contact laws. The properties of the primary constituents involved here, i.e., masonry, and the polymeric textile as provided by the manufacturer, are listed in Table 2. It should be noted that as is typically the case for polymer materials, the nominal specifications do not necessarily comply with the in-situ properties. A detailed outline of the further material properties of the stone building is provided in [18].

Table 2: Mechanical properties of the case-study materials.

Property	Masonry	Textile
Density	2579 kg/m^3	2000 kg/m^3
Young Modulus	$E = 2550$ MPa	$E_x = 40000$ MPa, $E_{y,z} = 32000$ MPa
Poisson Coefficient	$\nu = 0.4$	$\nu_{xy} = 0.14$, $\nu_{xz} = \nu_{yz} = 0.2$
Shear Modulus	840 MPa	4500 MPa
Maximum compression stress σ_c	3.28 MPa	
Maximum tensile stress σ_t	0.137 MPa	400 MPa
Maximum shear stress σ_s		10 MPa

Upon retrofitting with the polymeric textile, the building was assessed under seismic input on the Eucentre shake-table at increasing peak accelerations of 0.1g, 0.3g, 0.4g, 0.5g and 0.6g. The third test at 0.4g was in fact the first to induce damage and nonlinear response behavior. The resulting response was recorded via a set of accelerometers mounted in several positions on the structure.

4.1 Numerical – Experimental Characterization of the Composite Structure

The data recorded, by means of the described campaign, offer a multiplicity of information over various stages of the building's condition, namely prior to damage (URB), after damage-minor repair (DRB), and upon retrofitting with the polymeric textile (REB).

4.1.1 Step 1: Identification of Elastic Properties - OMA

In identifying the properties of the building in the elastic range for various condition stages, Operational Modal Analysis (OMA) may be employed [67]. OMA requires sets of ambient (broadband) vibration records on the basis of which modal properties, such as natural frequencies, mode shapes and damping ratios may be inferred. These were in this case extracted via four three-axis geophones, located on the parapet of the building's windows. Half-hour records were processed, acquired at a sampling rate of 265Hz per construction phase (URB, DRB, REB). In addition to the ambient records, forced hammer (impact) tests were further carried out, for corroborating the OMA results. The records were processed via use of well-established modal identification techniques, namely the Frequency Domain De-composition (FDD) and the Natural Excitation Technique combined with the Eigensystem Realization Algorithm (Next-ERA) [68, 69, 70]. The identified modal frequencies are summarized in Table 3 for the first three modes of the building.

Table 3: Experimental Modal Frequencies under Various Construction Phases

Mode #	URB Frequency [Hz]	DRB Frequency [Hz]	REB Frequency [Hz]
1	11.55	8.51	9.50
2	12.07	9.31	10.30
3	16.27	15.69	18.25

4.1.2 Step 2: Preliminary Numerical Analysis

A preliminary numerical Finite-Element-based model was set up in ANSYS [71]. The material properties were assigned according to the manufacturers specifications (Table 2 and [18]), while the modeling of damage and repairs was based on the close observation of the structure between construction phases. This included the recording of major crack patterns (size and orientation). Both masonry and the textile are in this preliminary simulation attempt modeled as anisotropic yet homogeneous materials. The first three modes identified via this rough numerical model are summarized in Table 5, where it is evident that the uncalibrated numerical model significantly overestimates the building's eigenfrequencies.

Table 4: Numerical Modal Frequencies under Various Construction Phases - no Model Calibration

Mode #	URB Frequency [Hz]	DRB Frequency [Hz]	REB Frequency [Hz]
1	12.62	10.93	13.77
2	13.51	12.28	14.73
3	20.22	19.25	22.35

While results do not appear significantly divergent for the first two modes of the unreinforced phase (URB), the error increases for the damaged/minor repairs phase (DRB), and it becomes quite significant for the retrofitted phase (REB). The discrepancy may be attributed to numerous uncertainties relating to lack of prior information, the simplifying assumptions in the modeling of the masonry and polymer constitutes, as well as the assumptions relating to the damage and intervention modeling (crack filling and diaphragm stiffening).

For ameliorating the estimation results, it is clear that a more refined approach need be enforced. At the same time, the nonlinear range of the response, available as part of the conducted shake-table tests, has not so far been exploited. In utilizing these results, a time history analysis is required, albeit implying significant computational toll. To this end, it is of the essence to utilize computational models, which may offer sufficient flexibility for the calibration (updating) process, while alleviating unreasonable computational toll owing to excessive refinement. Such a procedure is described next.

4.1.3 Step 3: Inverse Problem Formulation via Heuristic Optimization

In compromising the above-mentioned conflicting objectives, i.e., sophistication and model adaptability against computational cost, four different FE setups were put together corresponding to essentially four types of RVEs, as illustrated in Figure 7. The employed setups, which are materialized in ANSYS, correspond to varying modeling refinement levels, and therefore allow for diverse adaptability with respect to the actual case-study. More specifically,

Setup 1 (FE1)
In the first configuration masonry is discretized by means of an eight-noded solid element (SOLID65), which is capable of cracking/crushing and sliding (shear) effects across the crack face. The multiaxial textile is modeled as a homogeneous anisotropic material, with different properties along different wall faces, since walls placed perpendicular to the direction of the seismic load were dressed with more than one layers of textile. The SOLID46 layered element is adopted for the textile model, allowing for the combination of a layer of mortar (matrix) and a layer of the assumed anisotropic textile material. A total of 32 material parameters serve as inputs to be calibrated for this configuration.
Setup 2 (FE2)
In the second configuration masonry is once again modeled via SOLID65 elements. The textile is in this case approximated by a meso-scale representation, with the layered SOLID46 Finite Element now updated to include a total of 5 layers. The first layer corresponds to the mortar compound matrix, while the remaining four correspond to each one of the glass and polypropylene fiber layers, accounted for with their corresponding orientation angles. The fibers are represented via dedicated anisotropic materials. The different behavior along perpendicular wall directions is now accounted for via independent thickness parameters. A total of 31 material parameters serve as inputs to be calibrated for this configuration.
Setup 3 (FE3)
In the third configuration masonry is now discretized using the SOLID45 3D structural solid element, which allows for plasticity, creep, swelling, stress stiffening, large deflection, and large strain effects. It further accommodates anisotropic material properties, a feature which is not offered by the SOLID65 option used in the previous setups. The textile is modeled via the anisotropic macroscopic representation adopted in the 1st setup (FE1). A total of 39 material parameters serve as inputs to be calibrated for this configuration.
Setup 4 (FE4)
In the fourth configuration masonry is again modeled via the SOLID45 element, while the multi-axial reinforcing textile follows the meso-scale representation adopted in setup 2 (FE2). The total number of input parameters is now 40.

FE1 corresponds to the setup of the preliminary model, with the added option of calibrating the involved material properties. FE2 breaks the textile material further down to its constituents (meso-scale representation), permitting dedicated failure criteria per fiber class and orientation. This breakdown has been motivated from the mode of failure occurring during the shake-table tests, which lied along specific fibers and orientations. FE3 allows for refinement on the masonry front by introducing anisotropic properties for the masonry element. Finally, FE4 is the more refined modeling option, combining an anisotropic material for masonry and a meso-scale model for the textile.

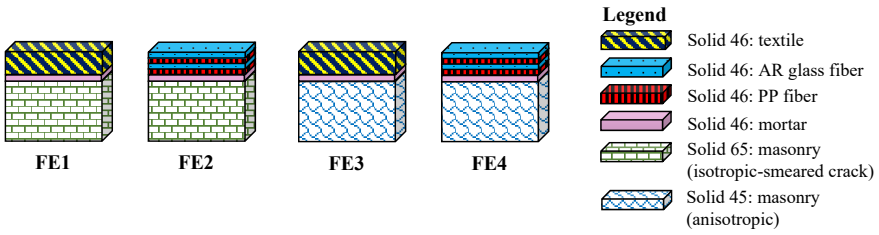

Fig. 7: Adopted FE Setups.

For updating the parameters of the candidate numerical models, a multistage evolutionary approach was implemented in [18]. A Genetic Algorithm (GA) is adopted as the heuristic optimization tool, albeit this being interchangeable with other alternatives, such as Particle Swarm Optimization (PSO) or the Covariance Matrix Adaptation Evolutionary Strategy algorithm (CMA-ES). A heuristic is deemed as appropriate for the inverse formulation discussed herein, due to lack of a straightforward functional relationship between the optimization function, i.e., the discrepancy between experiments and simulation, and the input parameters, i.e., the material properties. Given availability of a diverse set of reference (experimental) data, involving both Operational Modal Analysis & Nonlinear Dynamic tests across different construction phases of the case-study building, a multi-stage optimization procedure is set up. The unreinforced test data (URB) is discarded, given that damage essentially reinitializes the structural properties in the DRB case. The optimization process comprises the following stages:

Stage 1:
In this stage the elastic properties of the repaired masonry building (DRB) model are updated in order to yield an improved estimation, ω_s^{DRB}, of the experimentally identified frequencies, ω_e^{DRB}.

Stage 2:
In this stage, the experimentally identified frequencies of the Retrofitted Structure (REB) serve for updating the elastic properties of the textile on the basis

of the matching between experimental, ω_e^{REB}, and simulated, ω_s^{REB}, eigenfrequencies.
Stage 3:
While the former two analysis stages pertain to identification of elastic material properties, this stage performs a time history analysis. This allows for further configuration of the nonlinear material properties on the basis of the matching between experimental, a_e^i, and simulated, a_s^i, acceleration time histories in eight measured locations.

The final objective function (residual), r to be minimized via the GA occurs via superposition of the target approximations for each of the three aforementioned stages, and may be written as:

$$r = \frac{\left\|\omega_s^{DRB} - \omega_e^{DRB}\right\|}{\left\|\omega_e^{DRB}\right\|} + \frac{\left\|\omega_s^{REB} - \omega_e^{REB}\right\|}{\left\|\omega_e^{REB}\right\|} + \sum_{i=1}^{8} \frac{\left\|a_e^i - a_s^i\right\|}{\left\|a_e^i\right\|} \tag{18}$$

For all simulations ANSYS serves as the modeling platform, iteratively called from a Genetic Algorithm module coded in a Fortran environment [72].

4.1.4 Step 4: Updated Model Results

The convergence of the natural frequency approximation, during the GA-based optimization is presented in Figure 8 for each of the four candidate models, and contrasted to the experimentally identified values. The upper row of plots correspond to the damaged/repair (DRB) case, whilst the bottom row correspond to the modal estimates for the retrofitted (REB) case. The plots reveal that the updated modal estimates better approximate the experimental results, when contrasted against the preliminary (uncalibrated) model estimates (Table 3,5). Setups FE3 and FE4 return a closer approximation of the reference (experimental) values. This may be attributed to the higher flexibility of these setups; FE3 accounts for the anisotropic behavior of masonry, while FE4 achieves a more refined representation of the polymeric textile.

The third residual term, or optimization criterion, pertains to the approximation of the dynamic time history measurements, which further allows for calibration of the nonlinear material properties. Figure 9 illustrates results from FE4, which performs the best, from two characteristic building nodes (A & F), lying on the perimeter of the first and second floor of the structure respectively. Although not perfect, the simulation adequately approximates the observed dynamics. In further refining the achieved results, the material damping parameters ought to enter the optimization process, while the monitoring capability offered by the textile should be exploited. It is reminded that the textile features embedded fiber optic strain sensors, able to provide information on the micro-scale level.

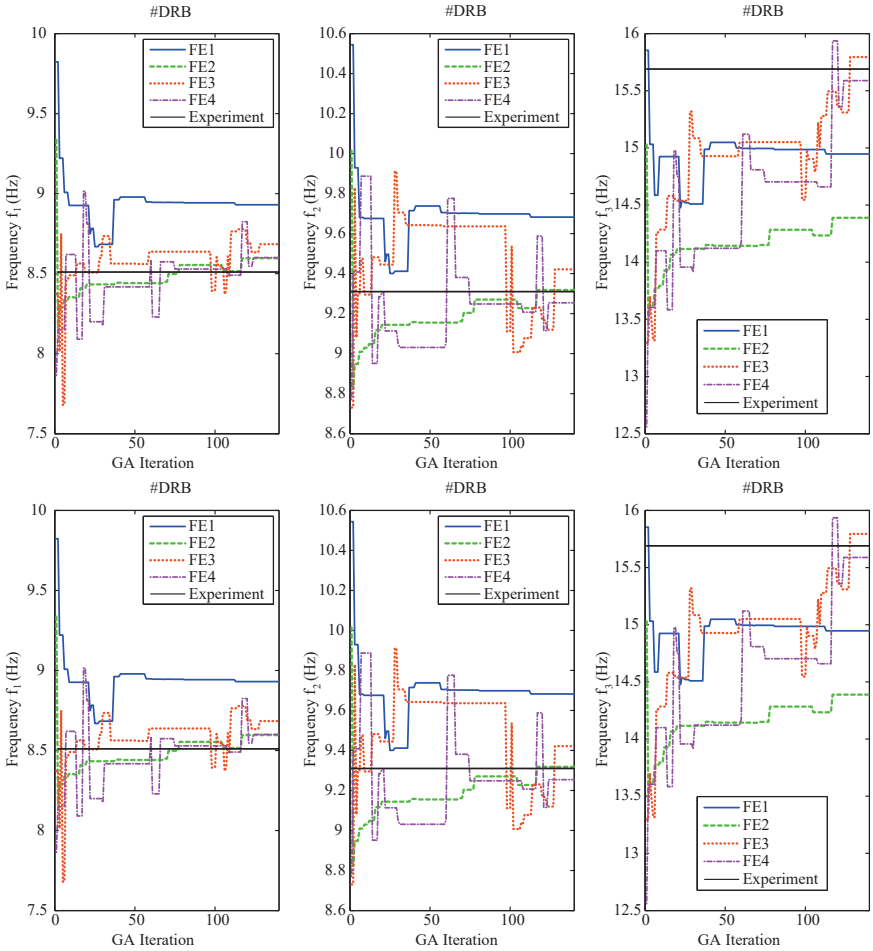

Fig. 8: Convergence plot for the candidate models (FE Setups) in terms of approximation of the elastic (eigenfrequency) properties of the damage/repaired (DRB-upper plots) and retrofitted (REB-lower plots) building.

However, the refinement of the simulation via introduction of further parameters into the optimization problem, or further refinement of the scale of the representation will eventually render the optimization procedure infeasible. The current modal analysis run-time lies in the order of ca. 10 sec against an order of ca. 15 min for the nonlinear dynamic analysis part (with the cost increasing for more complex FE setups). It is thus necessary to come up with efficient methods for accelerating the simulation procedure, particularly to what the dynamic nonlinear analysis component is concerned.

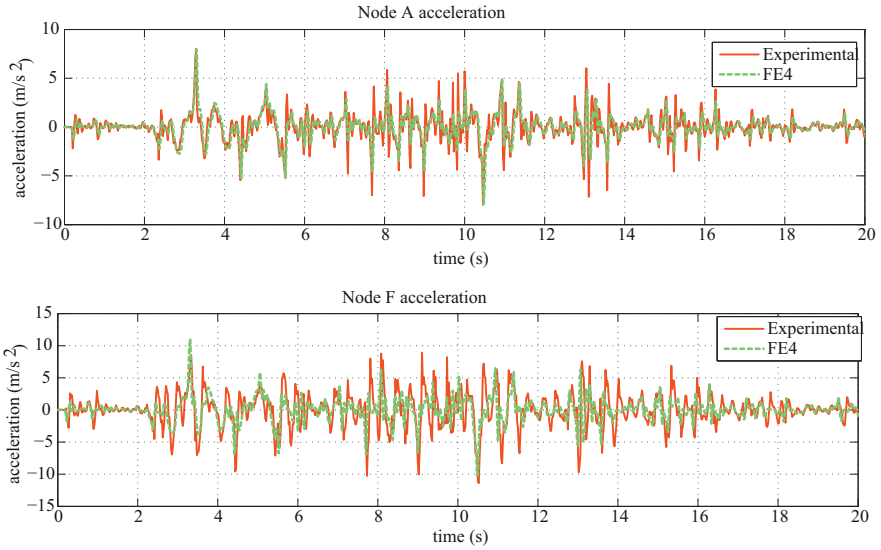

Fig. 9: Convergence plots for Setup FE4 in terms of approximation of the measured dynamic response of the damage/repaired (DRB-upper plots) and retrofitted (REB-lower plots) building offered at two characteristic locations.

5 Multiscale Analysis of Textile-Retrofitted Masonry Wall

As discussed in the earlier section, despite limiting the candidate models to meso-scale representations, a heavy computational toll occurs particularly with respect to the time history nonlinear analysis. The latter necessitates about 15 min for 10 sec of a single transient analysis, carried out on an average performance double core PC, versis only few seconds required by a modal analysis. Nonetheless, adoption of such an analysis is necessary when dynamic testing results are available, and identification of nonlinear properties is sought. In tackling this, Triantafyllou & Chatzi, introduced the HMsFEM discussed and overviewed in Section 3 [54]. The workings of the method have been demonstrated on the acceleration of the computation of polymer reinforced masonry structures in [57]. Following the construction stages outlined in the previous case-sudy, [57] overview the analysis of an unreinforced and textile-retrofitted masonry wall, this time by means of a multiscale FE based analysis. For details on the methodological front, the interested reader is referred to [57] for a thorough outline.

The cantilever masonry wall presented in Figure 10 is considered, comprising stone blocks, mortar and a single outer layer of textile-reinforcement in analogy to a single wall of the case-study presented in Section 4. The material properties are chosen in accordance to the previous case study, with addition of the properties of the smooth hysteretic law, which is now adopted for capturing the nonlinear behav-

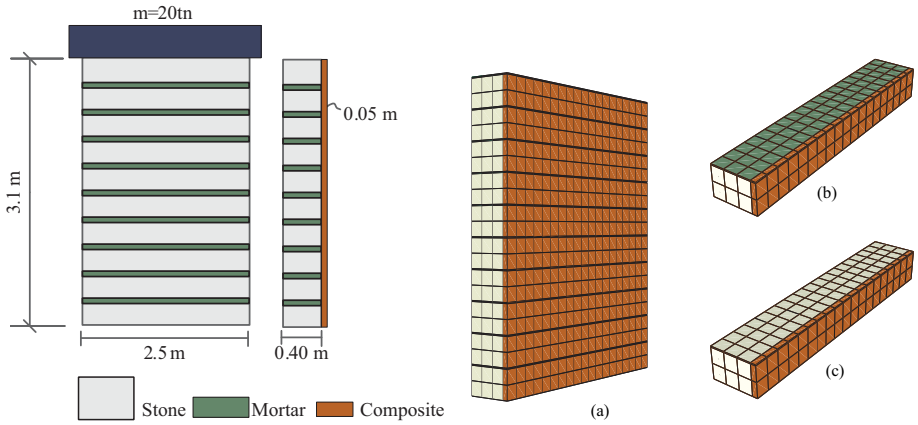

Fig. 10: Left: Textile-retrofitted masonry wall; Right: (a) Finite element model, (b) Multiscale model RVE#1, (c) Multiscale model RVE#2

ior. The textile, whose configuration follows the material employed in the previous case-study is modeled as a homogenized anisotropic layer (Figure 11). The elastic, plastic and hysteretic material properties of the constituents are summarized in Table 5.

Table 5: Multiscale Analysis Models - Constituent Material Properties

Parameters	Stone
Elastic/Plastic	$\rho_s = 1.8tn/m^3$, $E = 20.2$ GPa, $\sigma_c = 69.2$ MPa and $\sigma_t = 6.92$ MPa
Hysteretic Shape	$\beta = 0.1$, $\gamma = 0.9$, $N = 25$
Deterioration	$c_\eta = 0.002$ and $c_s = 0.005$
Parameters	**Mortar**
Elastic/Plastic	$\rho_m = 1.2tn/m^3$, $E = 3494MPa$, $\sigma_c = 3$ MPa, $\sigma_t = 0.3$ MPa Drucker-Prager dilation angle: $\psi = 60^o$
Hysteretic Shape	$\beta = \gamma = 0.5$, $N = 2$
Deterioration	$c_\eta = 0.002$ and $c_s = 0.05$
Pinching	$\zeta_1^0 = 1.0$, $\psi_0 = 0.05$, $\delta_\psi = 0.01$, $\mu = 0.0001$, $p = 1.2$, $q = 0.0001$
Parameters	**Polymeric Textile**
Elastic	$\rho_t = 2.0tn/m^3$, $E_{11} = 40$ GPa, $E_{22} = E_{33} = 32$ GPa, $E_{12} = E_{23} = E_{13} = 4.5$ GPa
Plastic	{wrap-knitted fibers: $\sigma_t = 10$ MPa, $\sigma_s = 400$ MPa}, {mortar matrix: $\sigma_c = 30$ MPa}
Hysteretic Shape	$\beta = 0.5$, $\gamma = 0.5$, $N = 25$
Deterioration	$c_\eta = 0.002$ and $c_s = 0.005$

The reference fine-meshed finite element model as illustrated in Figure 10a comprises 2223 hex–elements with full integration and 3020 nodes. The multiscale model instead features only 10 RVEs and 44 nodes, with two types of coarse el-

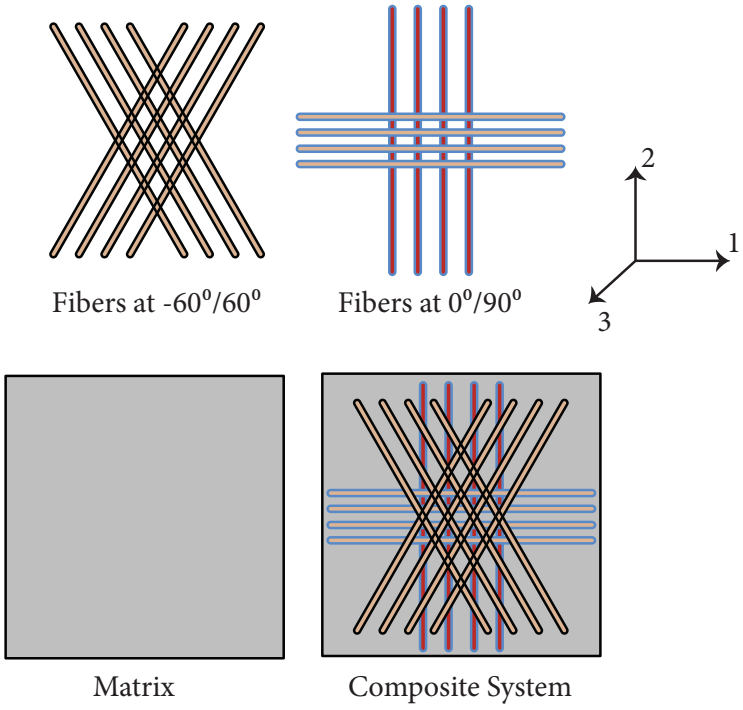

Fig. 11: Composition of the Polymeric Textile Reinforcement

ements of 228 micro-elements each (Figure 10b,c). The eigen-periods of the structure under consideration are $T_{in} = 0.19$ s and $T_{out} = 0.91$ s for the in-plane and out-of-plane eigen modes respectively.

A series of time-history analyses is then performed at a constant time step of dt = 0.001s. The unreinforced (URM) and retrofitted (REB) stages, i.e., the wall with and without textile, are subjected to seven unscaled ground motion records obtained from the PEER strong motion database [73] (Friuli, 1976;Victoria-Mexico, 1980; Northridge, 1995; Imperial Valley(E06), 1979; Chi-Chi, 1999; Imperial Valley(E07), 1979; Coyote Lake, 1979). The multiscale approach is verified in terms of accuracy against a conventional FE model built in ABAQUS [74], rendering a very good approximation. The analysis time for the ABAQUS FE model is ca. 125 min, while the multiscale analysis necessitates only 14 min, thereby offering an 88% acceleration in computation.

The derived in-plane displacement time-histories, calculated at the free end, are contrasted in Figures 12 (in-plane) and 13 (out-of-plane) for selected earthquake inputs in the URM and REB case. The peak displacements appear reduced for the REB case due to the strengthening functionality of the textile.

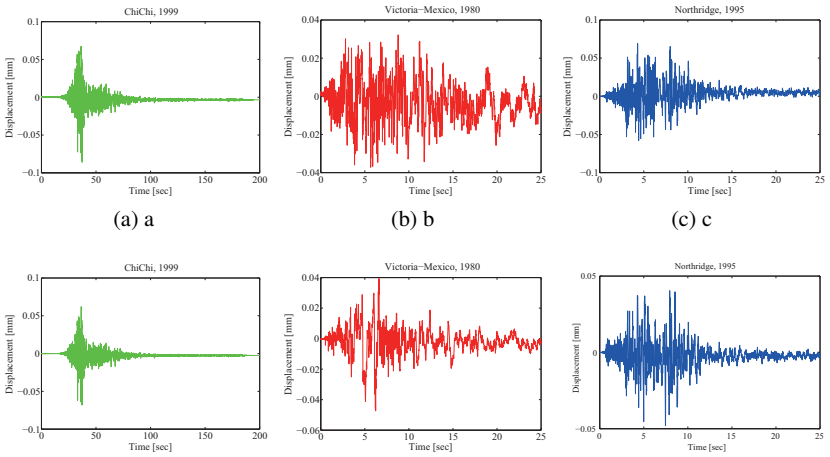

(a) a (b) b (c) c

(d) d (e) e (f) f

Fig. 12: In-plane Displacement Time Histories for the unreinforced (a,b,c) and retrofitted (e,d,f) case.

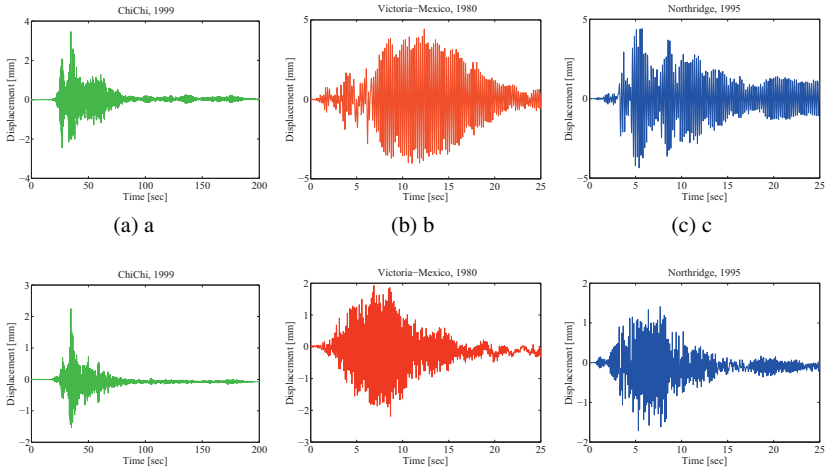

(a) a (b) b (c) c

(d) d (e) e (f) f

Fig. 13: Out-of-plane Displacement Time Histories for the unreinforced (a,b,c) and retrofitted (d,e,f) case.

A benefit of the multiscale approach is the continual interaction between the fine and coarse scale, which allows for estimating micro-scale quantities (such as local strains), as well as examining phenomena of damage accumulation at the micro-mesh level. By carrying out such an analysis, it appears that despite reduction in the experienced peak displacements, damage accumulation still occurs. This is evident in the hysteretic energy accumulation plot for the bottom mortar layer in Figure 14, albeit damage appears significantly reduced in the retrofitted case. Thus, although the textile composite layer succeeds in increasing the overall strength and stiffness of the masonry wall, it need be combined with conventional measures to ensure compliance with requirements at Damage Limitation performance level.

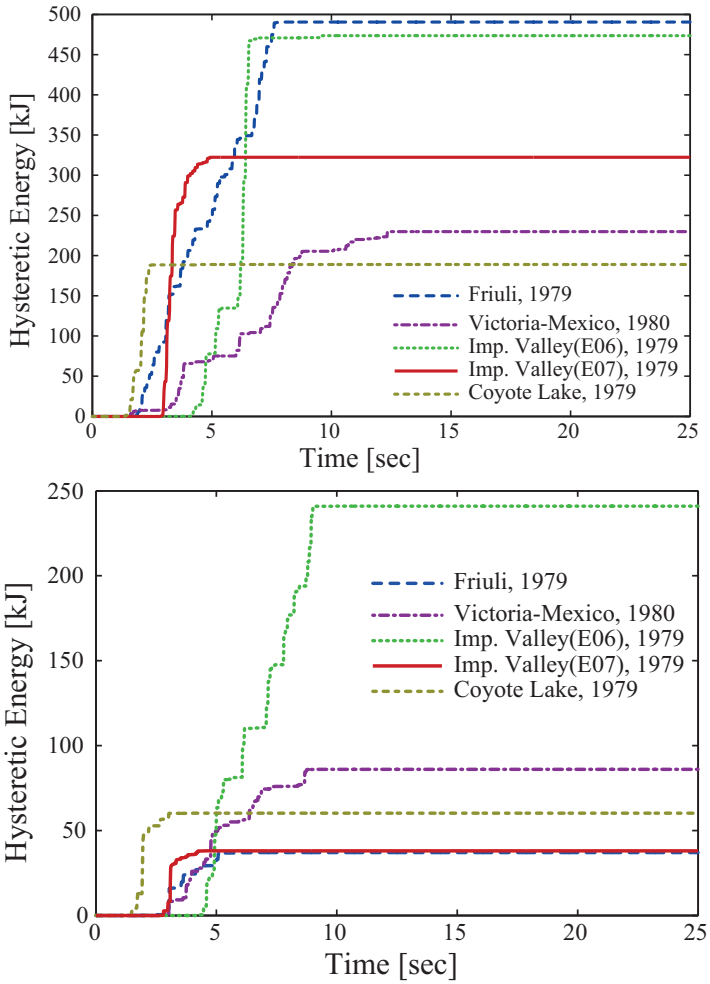

Fig. 14: Hysteretic energy accumulation at the bottom mortar layer, for the URM case (top); and the REB case (bottom).

The significant reduction in computation furnished by the HMsFEM scheme is particularly attractive with the context of an inverse analysis, as discussed in Section 4. Since the analysis time is reduced by an order of magnitude in this case, it would be feasible to consider implementation of identification techniques that are near-online, such as Kalman-type filters, as opposed to an offline optimization procedure, such as the GAs demonstrated earlier. This inverse problem formulation is overviewed in [60] where the HMsFEM scheme is coupled with an Unscented Kalman Filter for system identification under availability of sparse measurements.

6 Conclusions

Polymeric textiles comprise a highly effective solution for shielding cultural heritage structures, such as masonry or natural-stone buildings, from natural hazards and extreme events. Motivated by an extensive experimental campaign on the application of a polymeric textile full-cover solution on a natural-stone building, this work outlines numerical strategies that are required for i) the identification and characterization of the resulting composite structure in the elastic and plastic regime, and ii) the accelerated and multiscale simulation of such systems, for facilitating optimization, reliability and risk assessment tasks.

- Firstly, the experimental campaign and the measurements gathered within the context of the EU funded project Polymast are overviewed, carried out for different stages of the building's life (unreinforced, damaged/repaired and retrofitted). Subsequently, the aggregated measurements serve for updating, or fine-tuning, computational models of the masonry-textile composite system.
- Initially, a finite-element based analysis is performed, adopting configurations of varying refinement, and therefore fidelity. The numerical representations are maintained at a mesoscopic scale, in order to facilitate the coupling with computationally intensive schemes, such as heuristic optimization. It is shown that inclusion of refinement in the representation, increases the flexibility of the model and allows for a better tuning to the true system and the experimental results. Nonetheless, the analysis proves computationally costly, and almost prohibitive when cast in the context of condition and risk assessment, i.e., when approached from a probabilistic assessment viewpoint.
- To alleviate this issue, particularly when nonlinear dynamic analysis is required, the Hysteretic Multiscale FEM (HMsFEM) methodology, developed in previous works of the authors [54], is demonstrated as a viable reduced order model. The benefits of the proposed procedure are two-fold. i) On one hand, a significant reduction is achieved in the overall computation, in this case resulting in an order of magnitude decrease in overall analysis time. ii) On the other hand, and despite reduction in computation, precision and access to the information of the finer scale is maintained.

Naturally, the numerical scheme to be adopted should form a compromise between computational efficiency and complexity, which depends on the target of the simulation. The multiscale scheme discussed here is particularly meaningful when seeking to perform analyses which necessitate multiple iterations or multiple samples, as is often the case in risk and reliability assessment. Further benefits may be harnessed when this is coupled with monitoring technologies, which deliver not only global information, e.g. accelerations, but additionally local information, e.g. strains.

Acknowledgements Dr. Fuggini would like to gratefully acknowledge the support of European Community's Seventh Framework Programme [FP7/2007-2013] for access to Eucentre under grant agreement N 227887. Prof. Chatzi and Prof. Triantafyllou would like to gratefully acknowledge the support of the Swiss National Science Foundation under Research Grants #200021_146996, #200021_153379.

References

1. K. Thomas, *Masonry Walls: Specification and Design*. Butterworth Heinemann, Ofxord, 1996.
2. T. Salonikios, C. Karakostas, V. Lekidis, and A. Anthoine, "Comparative inelastic pushover analysis of masonry frames," *Engineering Structures*, vol. 25, no. 12, pp. 1515 – 1523, 2003.
3. T. J. Massart, R. H. J. Peerlings, and M. G. D. Geers, "An enhanced multi-scale approach for masonry wall computations with localization of damage," *Int. J. Numer. Meth. Engng.*, vol. 69, no. 5, pp. 1022–1059, 2007.
4. D. V. Oliveira, P. B. Lourenço, and P. Roca, "Cyclic behaviour of stone and brick masonry under uniaxial compressive loading," *Materials and Structures*, vol. 39, no. 2, pp. 247–257, 2006.
5. D. V. Oliveira, R. A. Silva, E. Garbin, and P. B. Lourenço, "Strengthening of three-leaf stone masonry walls: an experimental research," *Materials and Structures*, vol. 45, no. 8, pp. 1259–1276, 2012.
6. N. Mojsilović, "Strength of masonry subjected to in-plane loading: A contribution," *International Journal of Solids and Structures*, vol. 48, no. 6, pp. 865 – 873, 2011.
7. FEMA306, "Evaluation of earthquake damaged concrete and masonry wall buildings-basic procedures," *Technical Report, Federal Emergency Management Agency (FEMA), FEMA 306, Prepared by Applied Technology Council*, 1999.
8. T. Paulay and M. J. N. Priestly, *Seismic Design of Reinforced Concrete and Masonry Buildings*. John Wiley & Sons, Inc., 2009.
9. T. C. Triantafillou and M. N. Fardis, "Strengthening of historic masonry structures with composite materials," *Materials and Structures*, vol. 30, no. 8, pp. 486–496, 1997.
10. T. D. Krevaikas and T. C. Triantafillou, "Masonry confinement with fiber-reinforced polymers," *Journal of Composites for Construction*, vol. 9, no. 2, pp. 128–135, 2005.
11. T. Li, N. Galati, J. Tumialan, and A. Nanni, "Analysis of unreinforced masonry concrete walls strengthened with glass fiber-reinforced polymer bars," *ACI Structural Journal*, vol. 102, no. 4, pp. 569–577, 2005. cited By 14.
12. T. Triantafillou, *Textile-Reinforced Mortars (TRM)*, pp. 113–127. London: Springer London, 2011.
13. C. Faella, E. Martinelli, E. Nigro, and S. Paciello, "Tuff masonry walls strengthened with a new kind of c-frp sheet: experimental tests and analysis," in *Proceedings of the 13th world conference on earthquake engineering, paper no. 923.*, 2004.

14. A. Nurchi and M. Valdes, "Strengthening of stone masonry columns by means of cement-based composite wrapping," in *CCC 2005: 3rd international conference on composites in construction. Lyon, France, July 2005* (H. P, ed.), p. 11891196., 2005.
15. P. Bischof, R. Suter, E. Chatzi, and P. Lestuzzi, "On the use of cfrp sheets for the seismic retrofitting of masonry walls and the influence of mechanical anchorage," *Polymers*, vol. 6, no. 7, p. 1972, 2014.
16. T. Messervey, D. Zangani, and C. Fuggini, "Sensor-embedded textiles for the reinforce-ment, dynamic characterisation, and structural health monitoring of masonry structures," *Proceedings of the 5th EWSHM 2010, June 28July 2, Sorrento, Italy*, pp. 1075–1282, 2010.
17. L. Stempniewski, "Polyfunctional technical textiles for the protectionand monitoring of masonry structures against earthquakes," tech. rep., SEVENTH FRAMEWORK PROGRAMME, Capacities Specific Programme, Research Infrastructures, Project No.: 227887, 2011.
18. C. Fuggini, E. Chatzi, and D. Zangani, "Combining genetic algorithms with a meso-scale approach for system identification of a smart polymeric textile," *Computer-Aided Civil and Infrastructure Engineering*, vol. 28, no. 3, pp. 227–245, 2013.
19. C. Soares, M. de Freitas, A. Arajo, and P. Pedersen, "Identification of material properties of composite plate specimens," *Composite Structures*, vol. 25, no. 14, pp. 277 – 285, 1993.
20. P. Frederiksen, "Experimental procedure and results for the identification of elastic constants of thick orthotropic plates," *Journal of Composite Materials*, vol. 31, pp. 360–382, 1997.
21. R. Rikards, A. Chate, W. Steinchen, A. Kessler, and A. Bledzki, "Method for identification of elastic properties of laminates based on experiment design," *Composites Part B: Engineering*, vol. 30, no. 3, pp. 279 – 289, 1999.
22. J. Morton and G. Haig, *Designers' Guide to Eurocode 6: Design of Masonry Structures: EN 1996-1-1: General rules for reinforced and unreinforced masonry*. ICE Publishing, London., 2011.
23. L. Binda, J. Pina-Henriques, A. Anzani, A. Fontana, and P. Loureno, "A contribution for the understanding of load-transfer mechanisms in multi-leaf masonry walls: Testing and modelling," *Engineering Structures*, vol. 28, no. 8, pp. 1132 – 1148, 2006.
24. A. Anthoine, "In-plane behaviour of masonry: A literature review. report eur 13840 en, commission of the european communities," tech. rep., JRC - Institute for Safety Technology, Ispra, Italy, 1992.
25. P. Lourenco, *Computational strategies for masonry structures*. PhD thesis, Delft University of Technology, Delft, The Netherlands, 1996.
26. M. Tomazevic and M. Lutman, "Seismic behavior of masonry walls: Modeling of hysteretic rules," *Journal of Structural Engineering*, vol. 122, no. 9, pp. 1048–1054, 1996.
27. S.-Y. Chen, F. Moon, and T. Yi, "A macroelement for the nonlinear analysis of in-plane unreinforced masonry piers," *Engineering Structures*, vol. 30, no. 8, pp. 2242 – 2252, 2008. Seismic reliability, analysis, and protection of historic buildings and heritage sites.
28. M. A. R. Ferreira and H. K. H. Lee, "Multi-scale modeling: A bayesian perspective," *Springer Series in Statistics, New York: Springer*, 2007.
29. I. Babuška, "Homogenization approach in engineering," Tech. Rep. ORO–3443-58; TN-BN–828 United States; NSA-33-022692, 1975.
30. F. Nicot, F. Darve, R. G. N. Hazards, and V. of Structures, "A multi-scale approach to granular materials," *Mechanics of Materials*, vol. 37, no. 9, pp. 980 – 1006, 2005.
31. M. S. Elsayed and D. Pasini, "Multiscale structural design of columns made of regular octet-truss lattice material," *International Journal of Solids and Structures*, vol. 47, no. 1415, pp. 1764 – 1774, 2010.
32. K. Mangipudi and P. Onck, "Multiscale modelling of damage and failure in two-dimensional metallic foams," *Journal of the Mechanics and Physics of Solids*, vol. 59, no. 7, pp. 1437 – 1461, 2011.
33. D. L. McDowell, "A perspective on trends in multiscale plasticity," *International Journal of Plasticity*, vol. 26, no. 9, pp. 1280 – 1309, 2010. Special Issue In Honor of David L. McDowell.
34. T. J. Hughes, G. Scovazzi, P. B. Bochev, and A. Buffa, "A multiscale discontinuous galerkin method with the computational structure of a continuous galerkin method," *Computer Methods in Applied Mechanics and Engineering*, vol. 195, no. 1922, pp. 2761 – 2787, 2006.

35. J.-H. Song and T. Belytschko, "Multiscale aggregating discontinuities method for micromacro failure of composites," *Composites Part B: Engineering*, vol. 40, no. 6, pp. 417 – 426, 2009. Blast/impact on engineered (nano)composite materials.
36. P. Kanouté, D. P. Boso, J. L. Chaboche, and B. A. Schrefler, "Multiscale methods for composites: A review," *Archives of Computational Methods in Engineering*, vol. 16, no. 1, pp. 31–75, 2009.
37. T. Belytschko and R. de Borst, "Multiscale methods in computational mechanics," *International Journal for Numerical Methods in Engineering*, vol. 83, no. 8-9, pp. 939–939, 2010.
38. X. Xu and L. Graham-Brady, "A stochastic computational method for evaluation of global and local behavior of random elastic media," *Computer Methods in Applied Mechanics and Engineering*, vol. 194, no. 4244, pp. 4362 – 4385, 2005.
39. M. Tootkaboni and L. Graham-Brady, "A multi-scale spectral stochastic method for homogenization of multi-phase periodic composites with random material properties," *International Journal for Numerical Methods in Engineering*, vol. 83, no. 1, pp. 59–90, 2010.
40. X. F. Xu, K. Hu, I. J. Beyerlein, and G. Deodatis, "Statistical strength of hierarchical carbon nanotube composites," *International Journal for Uncertainty Quantification*, vol. 1, no. 4, pp. 279–295, 2011.
41. T. Massart, R. Peerlings, and M. Geers, "Mesoscopic modeling of failure and damage-induced anisotropy in brick masonry," *European Journal of Mechanics - A/Solids*, vol. 23, no. 5, pp. 719 – 735, 2004.
42. T. Massart, R. Peerlings, M. Geers, and S. Gottcheiner, "Mesoscopic modeling of failure in brick masonry accounting for three-dimensional effects," *Engineering Fracture Mechanics*, vol. 72, no. 8, pp. 1238 – 1253, 2005.
43. Y. Efendiev and T. Y. Hou, *Multiscale Finite Element Methods*, vol. 4 of *Surveys and Tutorials in the Applied Mathematical Sciences*. Springer, 2009.
44. H. W. Zhang, J. K. Wu, and J. Lv, "A new multiscale computational method for elasto-plastic analysis of heterogeneous materials," *Computational Mechanics*, vol. 49, no. 2, pp. 149–169, 2012.
45. L. Karapitta, H. Mouzakis, and P. Carydis, "Explicit finite-element analysis for the in-plane cyclic behavior of unreinforced masonry structures," *Earthquake Engineering & Structural Dynamics*, vol. 40, no. 2, pp. 175–193, 2011.
46. Y. Wen, "Method of random vibration of hysteretic systems," *Journal of Engineering Mechanics Division*, vol. 102, pp. 249–263, 1976.
47. I. Mayergoyz, "Generalized preisach model of hysteresis," *IEEE Transactions on Magnetics*, vol. 24, no. 1, pp. 212–217, 1998.
48. S. Erlicher and O. S. Bursi, "Boucwen-type models with stiffness degradation: Thermodynamic analysis and applications," *Journal of Engineering Mechanics*, vol. 134, no. 10, pp. 843–855, 2008.
49. M. V. Sivaselvan and A. M. Reinhorn, "Hysteretic models for deteriorating inelastic structures," *Journal of Engineering Mechanics*, vol. 126, no. 6, pp. 633–640, 2000.
50. A. Visintin, "Differential models of hysteresis," in *Applied Mathematical Sciences*, vol. 111, Springer,, 1994.
51. F. Ikhouane and J. Rodellar, *Systems with hysteresis: Analysis, identification and control using the Bouc-Wen model*. John Wiley & Sons, New York, 2007.
52. P. D. Spanos and I. A. Kougioumtzoglou, "Harmonic wavelet-based statistical linearization of the Bouc-Wen hysteretic model," pp. 2649–2656, Taylor and Francis Group, 2011.
53. S. P. Triantafyllou and V. K. Koumousis, "A hysteretic quadrilateral plane stress element," vol. 82, no. 10-11, pp. 1675–1687, 2012.
54. S. Triantafyllou and E. Chatzi, "A hysteretic multiscale formulation for nonlinear dynamic analysis of composite materials," *Computational Mechanics*, vol. 54, no. 3, pp. 763–787, 2014.
55. O. C. Zienkiewicz, R. L. Taylor, and J. Zhu, *The Finite Element Method: Its Basis and Fundamentals*. Elsevier, Amsterdam, 6 ed., 2005.
56. S. Triantafyllou and E. Chatzi, *Risk Analysis of Composite Structures by Subset Estimation Using the Hysteretic Multiscale Finite Element Method*, ch. 157, pp. 1564–1573. 2014.

57. S. P. Triantafyllou and E. N. Chatzi, *Towards a Multiscale Scheme for Nonlinear Dynamic Analysis of Masonry Structures with Damage*, pp. 165–198. Cham: Springer International Publishing, 2015.
58. S. Nemat-Naser, "On finite deformation elasto-plasticity," *International Journal of Solids and Structures*, vol. 18, no. 10, pp. 857–872, 1982.
59. K. Washizu, *Variational Methods in Elasticity and Plasticity*. Pergamon Press, Oxford, 1983.
60. S. P. Triantafyllou and E. N. Chatzi, "A hysteretic multiscale formulation for validating computational models of heterogeneous structures," *The Journal of Strain Analysis for Engineering Design*, 2015.
61. W. D. Iwan, "On a class of models for the yielding behavior of continuous and composite systems," *Journal of Applied Mechanics*, vol. 34, no. 3, pp. 612–617, 1967.
62. S. Erlicher, *Hysteretic degrading models for the low-cycle fatigue behaviour of structural elements: theory, numerical aspects and applications*. PhD thesis, Department of Mechanical and Structural Engineering, University of Trento, Italy, 2003.
63. S. Triantafyllou and V. Koumousis, "Hysteretic finite elements for the nonlinear static and dynamic analysis of structures," *Journal of Engineering Mechanics*, vol. 140, no. 6, pp. 04014025–1– 04014025–17, 2014.
64. J. Lubliner, *Plasticity Theory*. New York: Dover Publications, 2008.
65. G. C. Foliente, M. P. Singh, and M. N. Noori, "Equivalent linearization of generally pinching hysteretic and degrading systems," *Earthquake Engineering & Structural Dynamics*, vol. 25, pp. 611–629, 1996.
66. D. Zangani, "Final report - polytect (polyfunctional technical textiles against natural hazards), project no. nmp2-ct-2006-026789," tech. rep., D' Appolonia S.p.A, 2010.
67. B. Peeters and G. De Roeck, "Stochastic system identification for operational modal analysis: A review," *Journal of Dynamic Systems, Measurement, and Control*, vol. 123, pp. 659–667, Feb. 2001.
68. G. H. James, T. G. Carne, J. P. Lauffer, and A. R. Nord, "Modal testing using natural excitation," *Proceedings of 10th Int. Modal Analysis Conference, San Diego*, 1992.
69. J.-N. Juang and R. S. Pappa, "An eigensystem realization algorithm for modal parameter identification and model reduction," *Journal of Guidance, Control, and Dynamics*, vol. 8, pp. 620–627, Sept. 1985.
70. R. Brincker, L. Zhang, and P. Andersen, "Modal identification from ambient responses using frequency domain decomposition," *Proceedings of the 18th SEM International Modal Analysis Con-ference, San Antonio*, 2000.
71. "Ansys academic research, release 16.2."
72. "D. l. carrols open source code: http://www.cuaerospace.com/carroll/ga.html."
73. "http://peer.berkeley.edu/peer_ground_motion_database/. accessed 20 may 2014."
74. "Ri. abaqus version 6.11 [computer software]. dassault systmes simulia, providence.."